Magnetic properties and electronic structures of R–Ni–B compounds where R is a heavy rare earth

2008 J. Phys.: Condens. Matter 20 275201

(http://iopscience.iop.org/0953-8984/20/27/275201)

J. Phys.: Condens. Matter **20** (2008) 275201 (7pp) doi:10.1088/0953-8984/20/27/275201

Magnetic properties and electronic structures of R–Ni–B compounds where R is a heavy rare earth

E Burzo[1], N Bucur[1], L Chioncel[2,3] and V Rednic[1]

[1] Faculty of Physics, Babes-Bolyai University, 400084 Cluj-Napoca, Romania
[2] Institute of Theoretical Physics, Graz University of Technology, A-8010 Graz, Austria
[3] Department of Physics, University of Oradea, RO-410087, Oradea, Romania

Received 11 February 2008, in final form 18 April 2008
Published 2 June 2008
Online at stacks.iop.org/JPhysCM/20/275201

Abstract
Magnetic measurements were performed in the temperature range 4.2–300 K and fields up to 70 kOe on $R_3Ni_7B_2$ compounds with R = Gd, Tb, Dy, Ho, Er. The Curie temperatures decrease from 38.5 K (Gd) to 7 K (Er). Band structure calculations show that nickel, at 0 K, has a very small magnetic polarization, oriented antiparallel to the rare-earth moment. The XPS measurements suggest the presence of unoccupied Ni3d states. The reciprocal susceptibilities follow a Curie–Weiss type behaviour. Effective nickel moments of $1.33 \pm 0.25\ \mu_B$ were determined. The magnetic behaviour of nickel is analysed in models which take into account electron correlation effects in d bands.

(Some figures in this article are in colour only in the electronic version)

1. Introduction

The magnetic behaviour of nickel in rare-earth (R) compounds has been a subject of debate. As an example, the nickel in RNi_5 and RNi_2 compounds was for a long time considered to be nonmagnetic [1]. Later on, analysing the magnetic properties of $(Gd_xY_{1-x})Ni_5$ [2] and $(Gd_xLa_{1-x})Ni_5$ [3] systems, at 1.7 K, it was shown that nickel is not magnetically ordered in $LaNi_5$ and YNi_5 and an induced moment appears when La or Y were replaced by Gd. In RNi_5 compounds with magnetic rare-earths, nickel shows also a magnetic ordered moment. When both R and Ni are magnetic, there is evidence of 4f–5d–3d and 5d–5d exchange interactions [4].

Band structure calculations, performed on RNi_2 compounds, with magnetic heavy rare-earths, showed that a nickel moment is still present at 0 K and is oriented antiparallel to the rare-earth one [5]. As an example, in $GdNi_2$ a spin moment of 0.12 μ_B/Ni atom was computed. This behaviour was later confirmed by using the magnetic Compton profile method [6]. A spin moment of $0.16 \pm 0.08\ \mu_B$ and a total magnetic moment of $0.23 \pm 0.11\ \mu_B$/Ni atom was reported. A Gd5d band polarization of 0.29 μ_B/atom, oriented parallel to the Gd4f moment, was determined in $GdNi_2$. This contribution is cancelled by the magnetic moments of the two nickel atoms, resulting in a magnetization of 7 μ_B per formula unit, similar to that evidenced by magnetic measurements.

In an on-going work on the magnetic properties of R–Ni compounds, we studied the $R_3Ni_7B_2$ system. In addition to magnetic measurements, x-ray photoelectron spectroscopy studies and band structure calculations were also performed. The crystal structure of $R_3Ni_7B_2$ compounds, where R is heavy rare earth, was previously reported [7]. The compounds crystallize in a hexagonal $P6_3/mmc$ type lattice. The R atoms occupy 2c and 4f sites and Ni atoms are situated in 2a and 12k positions. Boron atoms are distributed on 2b and 2d type sites.

2. Experimental and computing method

The $R_3Ni_7B_2$ (R = Gd, Tb, Dy, Ho, Er) compounds were prepared by arc melting the constituent elements in a purified argon atmosphere. The compounds were thermally treated at 850 °C for one week. The x-ray analyses show the presence of only one phase. The compounds crystallize in a hexagonal type structure—figure 1. The lattice parameters are listed in table 1. These are close to the values previously reported [7].

The magnetic measurements were performed in the temperature range 4.2–300 K and fields up to 70 kOe. The saturation magnetizations, M_s, were obtained, according to the approach of the saturation law, $M = M_s(1 - a/H)$, by extrapolating the measured values, M, at $H^{-1} \to 0$; a denotes the coefficient of magnetic hardness.

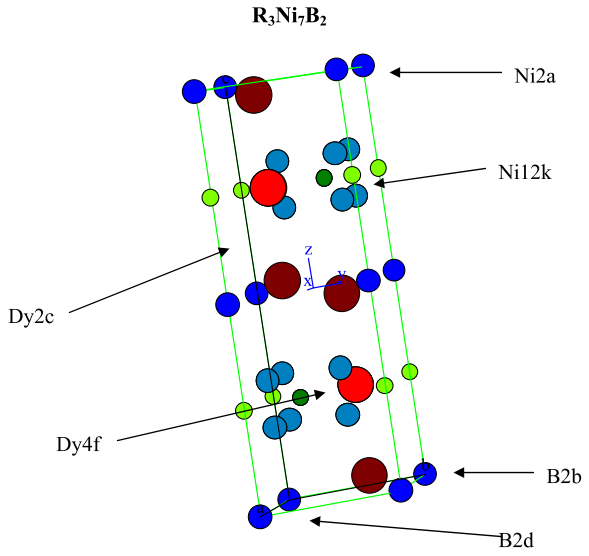

Figure 1. Crystal structure of $R_3Ni_7B_2$ compounds. In $P6_3/mmc$ type lattice, two types of sites are present for R, Ni, and B atoms.

XPS measurements were performed by using a PH5 5000 MultiTechnique System. All the spectra were recorded at room temperature, using monochromatized Al Kα radiation (1486.6 eV). The total resolution, as determined at the Fermi level of a gold foil, was about 0.3–0.4 eV. The binding energies are given with reference to the Fermi level. The $4f_{7/2}$ level of gold was found at 84.0 eV binding energy. The samples were fracturated in a preparation chamber. All spectra were recorded in vacuum below 5×10^{-10} mbar. The fracturated samples contained only tiny amounts of oxygen and carbon.

The band structure calculations were performed by using as a basic framework the density functional theory (DFT), in combination with three different schemes: (1) itinerant 4f electrons using the local density approximation; (2) fully localized 4f, putting them in the core and (3) partially localized 4f electrons by using the LSDA + U approximation. For localized 4f electrons we have employed the open–core approach [8, 9]. The local-spin density approximation (LSDA) as well as the LSDA + U approach were used when the 4f electrons were considered in the band. In the LSDA + U approach an intra-atomic Coulomb interaction, U, was added. Here we adopted the around-mean field (AMF) form of the so-called LSDA + U double counting term [10]. For rare-earths, the average Coulomb interaction U_f = 7–8 eV and exchange interaction J_f = 1 eV were chosen to reproduce experimental data, as previously reported [11]. For nickel, values U_d = 2 eV and J_d = 0.9 eV, which are widely accepted [12], were used.

3. Band structures

The total and partial densities of states of $R_2Ni_7B_3$ compounds with R = Gd, Tb, Dy, and Ho, computed by considering the R4f states in core, as well those obtained by LSDA + U approximation are plotted in figure 2. The band structure of $Gd_2Ni_7B_3$ obtained in the LSDA approach is also given. In the last case, the occupied 4f bands are located at 3.5–4.5 eV below the Fermi level and the empty states above, but close to the Fermi level. This arrangement is not supported by the real band structures and leads to a nonphysical result due to a strong 3d–4f hybridization. Thus, in the following we analyse comparatively only the data obtained from band structure calculations when using the LSDA + U approximation and when the 4f states were in the core.

Table 1. Lattice parameters at room temperature.

Compound	a (Å)	c (Å)	V (Å^3)
$Gd_3Ni_7B_2$	5.115(2)	14.342(1)	324.51
$Tb_3Ni_7B_2$	5.097(2)	14.335(1)	322.52
$Dy_3Ni_7B_2$	5.080(5)	14.315(4)	320.01
$Ho_3Ni_7B_2$	5.051(9)	14.307(5)	316.25
$Er_3Ni_7B_2$	5.045(1)	14.248(3)	314.10

The computed nickel moments, M_{Ni} are small and oriented antiparallel to those of the rare-earths. These are linearly dependent on the De Gennes factor, $G = (g_J - 1)^2 J(J + 1)$, suggesting that they essentially are induced through a 4f–5d–3d exchange path—figure 3. The M_{Ni} values, as obtained when the 4f states were considered in the core or by using the LSDA + U method, are very close. In both methods, the Ni2a moments are higher than those of nickel located in the 12k sites. This behaviour can be correlated with their different crystallographic environments. There is a stronger hybridization of Ni3d and B2p bands, at Ni12k sites, as a result of closer distance between these atoms. In addition, the 4f–5d–3d exchange interactions are not so strong due to the smaller number of R atoms located in their near neighbourhood, as compared to Ni2a sites.

The R5d bands are polarized and their magnetic contributions, M_{5d}, are oriented parallel to R4f moments. A linear dependence on the De Gennes factor is also shown. Nearly the same M_{5d} polarizations are obtained for both R sites, showing that the local environments have little influence on these values—figure 4. This behaviour can be correlated with the same number of nickel atoms (12) situated in their first coordination shells. No significant differences are obtained when using the LSDA + U method or considering the 4f states in the core.

The extrapolation of M_{5d} versus G values, at $G = 0$, shows the presence of a small polarization, $M_{5d}(0) = 0.07\ \mu_B$. The $M_{5d}(0)$ value can be correlated with induced polarization due to 5d–3d short range exchange interactions, as previously shown in the $(Gd_xLa_{1-x})Ni_5$ system [4].

The comparative analysis of the above data shows that the LSDA + U approximation leads to more reliable results by also taking into account the contributions of 4f states to electronic structure.

4. XPS measurements

The $Ni2p_{3/2}$ and $Ni2p_{1/2}$ core level lines in $R_3Ni_7B_2$ (R = Gd, Tb, Dy) compounds are plotted in figure 5, together with those of pure nickel [13]. The main features of the $R_3Ni_7B_2$ spectra reproduce well those of pure nickel. The binding energies of $Ni2p_{3/2}$ and $Ni2p_{1/2}$ core level lines of pure nickel are situated

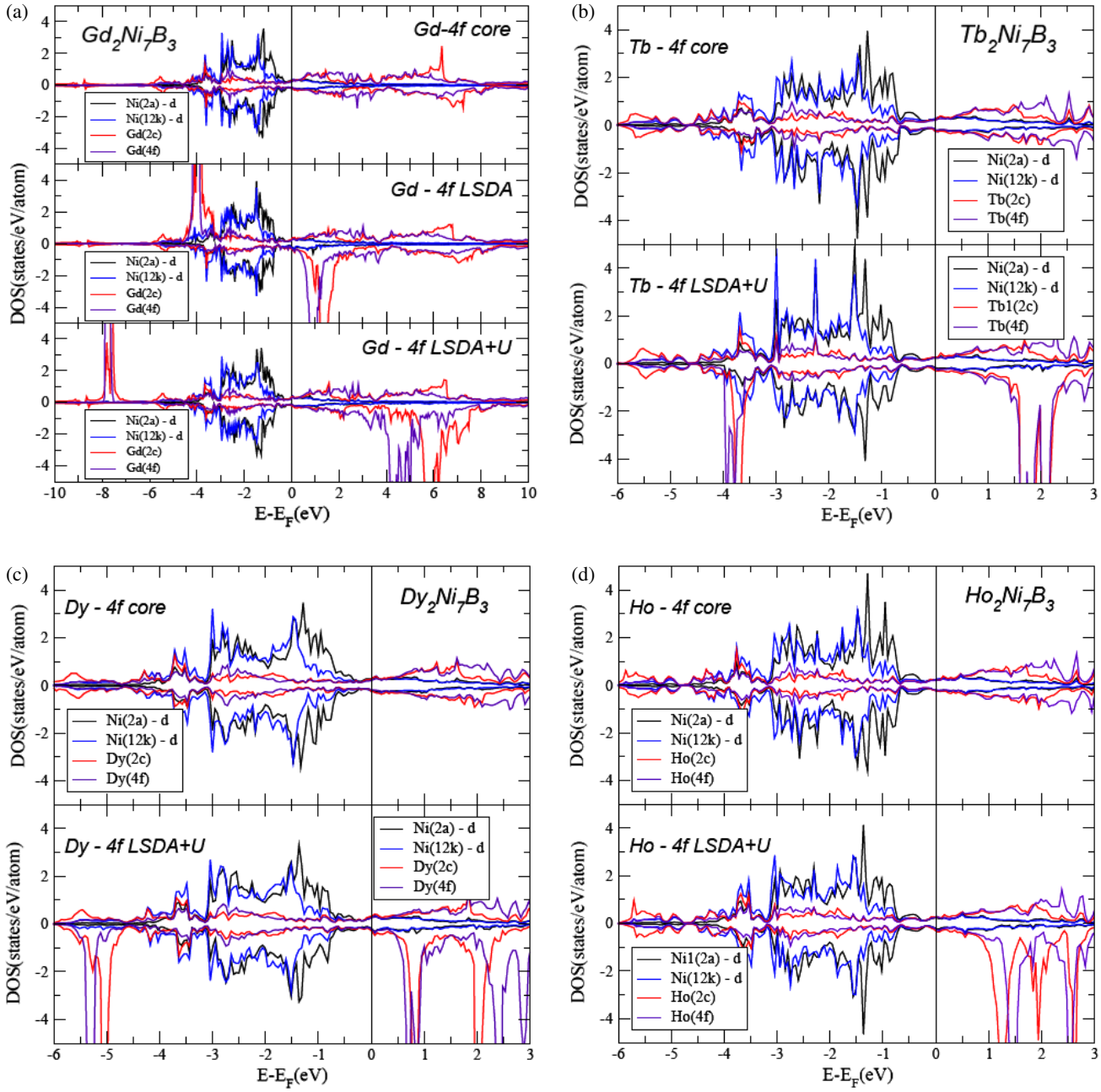

Figure 2. Total and partial densities of states for $R_2Ni_7B_3$ compounds with R = Gd, Tb, Dy, and Ho. The band structures obtained when 4f electrons were considered in the core as well in the LSDA + U approximation are plotted: (a) $Gd_2Ni_7B_3$ ($U_f = 7$ eV, $J_f = 1$ eV). (b) $Tb_2Ni_7B_3$ ($U_f = 7$ eV, $J_f = 1$ eV); (c) $Dy_2Ni_7B_3$ ($U_f = 7$ eV, $J_f = 1$ eV); (d) $Ho_2Ni_7B_3$ ($U_f = 8$ eV, $J_f = 1$ eV). For nickel, values $U_d = 2$ eV, $J_d = 0.9$ eV were used. In (a) the band structure of $Gd_2Ni_7B_3$ obtained by using the LSDA method is also given.

at 852.7 ± 0.1 and 869.97 ± 0.1 eV [13]. Values 852.85 ± 0.05 and 870.05 ± 0.05 were shown in $R_3Ni_7B_2$ compounds. Thus, these lines are shifted by no more than $\cong$0.1 eV, at higher binding energies, as compared to pure nickel. In all the compounds, the 6 eV satellite lines are present, although their intensities are decreased as compared to pure nickel. The above feature suggests, at room temperature, the presence of unoccupied Ni3d states, although their number is diminished relative to that of nickel.

The R4d core level lines of $R_3Ni_7B_2$ compounds with R = Gd, Tb, Dy are shown in figure 6. The Dy4d lines are located at 152, 155.4, and 157 eV binding energies, the same as in Dy metal [13]. Similar behaviour is also shown for Tb4d core level lines in $Tb_3Ni_7B_3$, which are situated at 146.3, 150, and 152.5 eV. In the case of $Gd_3Ni_7B_2$, the Gd4d line located at 142.3 eV has a large linewidth. This is an envelope of the three narrow lines situated in the pure Gd spectrum between 141.5 and 143.5 eV [13]. The peak at 147.3 eV is located at the same energy as in Gd metal. We conclude that the R4d lines are located at the same binding energies as in the pure R metals. The somewhat larger linewidths in $R_3Ni_7B_2$ compounds as well as the presence of an envelope for closed

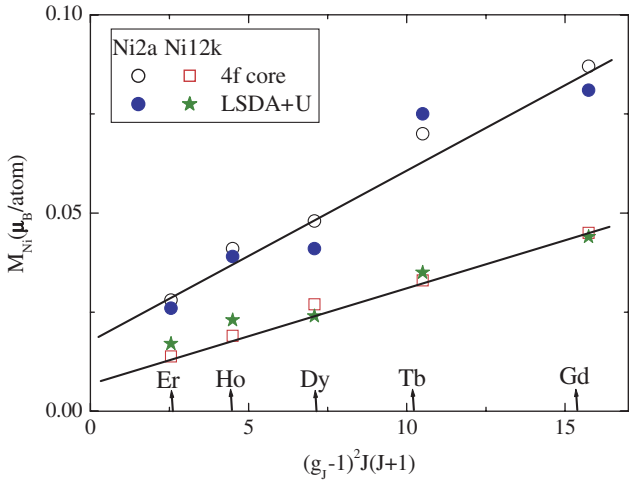

Figure 3. Computed nickel moments at 2a and 12k sites as a function of the De Gennes factor.

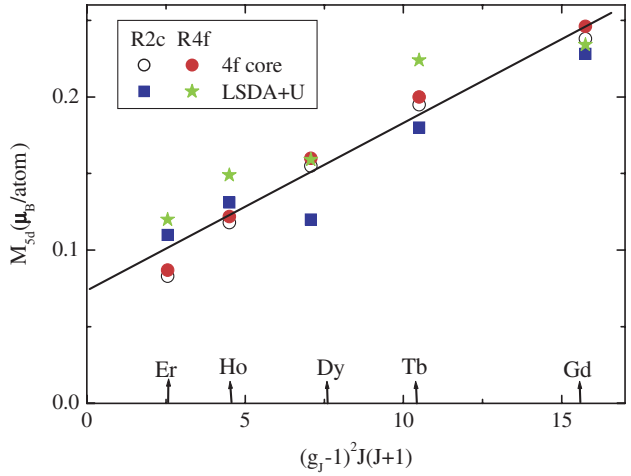

Figure 4. Computed R5d band polarizations at 2c and 4f sites as a function of the De Gennes factor.

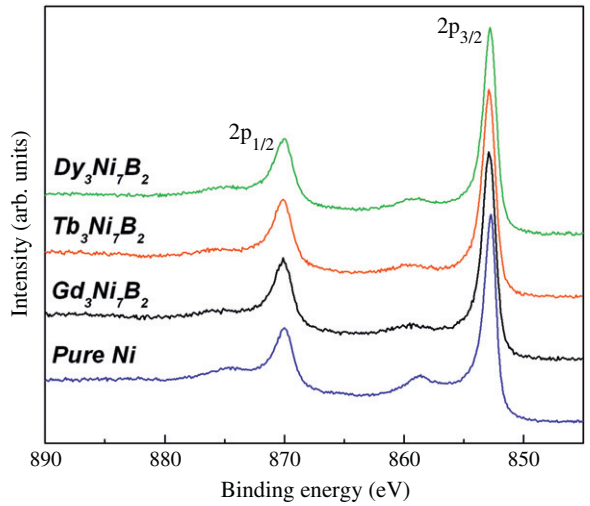

Figure 5. The $Ni2p_{3/2}$ and $Ni2p_{1/2}$ core level lines in $R_3Ni_7B_2$ (R = Gd, Tb, Dy) compounds and pure nickel.

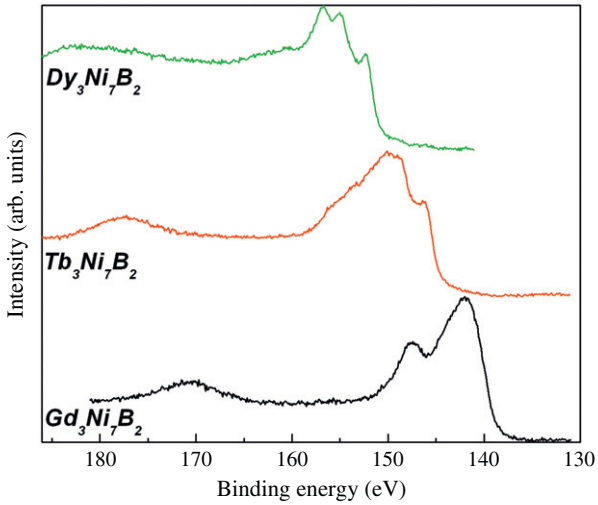

Figure 6. The R4d core level lines in $R_3Ni_7B_2$ compounds (R = Gd, Tb, Dy).

lines situated around 142.3 eV, in $Gd_3Ni_7B_2$, can be correlated with the presence of two types of R sites in $P6_3/mmc$ type lattice. The corresponding binding energies are expected to be very close, and only a broadening of lines can be shown.

The $R3d_{3/2}$ and $R3d_{5/2}$ core level lines in the case of $R_3Ni_7B_2$ (R = Gd, Tb, Dy) compounds are shown in figure 7. These lines are only slightly shifted to higher binding energies compared to the respective lines of pure metals [13].

The XPS valence band spectra of $R_3Ni_7B_2$ compounds as well as of pure nickel are shown in figure 8. The $R_3Ni_7B_2$ spectra are the result of superposition of those characteristic of R and Ni. The valence band spectrum of pure nickel shows a main line located at ≅0.6 eV binding energy and the 6 eV satellite [13]. The Ni3d lines in $R_3Ni_7B_2$ compounds are broadened and thus the positions of the maxima cannot be precisely determined. From the analysis of the spectra we estimated a shift of the main lines at higher energies by ≅0.3 eV as compared to pure nickel. Due to the relatively low intensities, as well as to the superposition with the R4f bands, the 6 eV satellites cannot be identified. The densities of states, at the Fermi level, are diminished as compared to the nickel ones, in agreement with band structure calculations. The 4f orbitals of rare-earths in $R_3Ni_7B_2$ compounds keep their localized character and therefore the XPS band spectra show multiplet structures. These correspond to transitions between the ground state having $4f^n$ configuration, to the accessible final states of $4f^{n-1}$ configurations. As an example, the experimental spectrum of dysprosium metal was decomposed in nine lines mainly attributed to $Dy4f_{7/2}$ and $Dy4f_{5/2}$ [13]. The more intense lines are located at binding energies of 4.0 eV (16.97%), 7.8 eV (29.02%), and 9.27 eV (23.47%). The line intensities of Dy metal were also theoretically calculated [14–17]. A rather good agreement with the experimental spectrum was obtained by Lang *et al* [16]. Assuming that the positions of Dy4f lines in $R_3Ni_7B_2$ compounds, situated at higher binding energies, are not much influenced by the superposition effects,

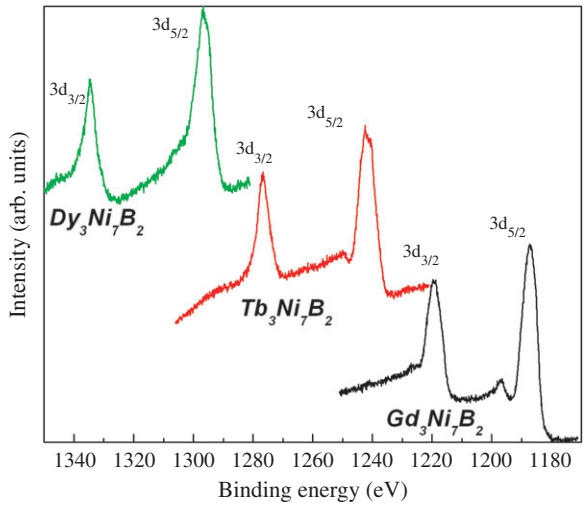

Figure 7. The R3d$_{5/2}$ and R3d$_{3/2}$ core level lines in $R_3Ni_7B_2$ compounds (R = Gd, Tb, Dy).

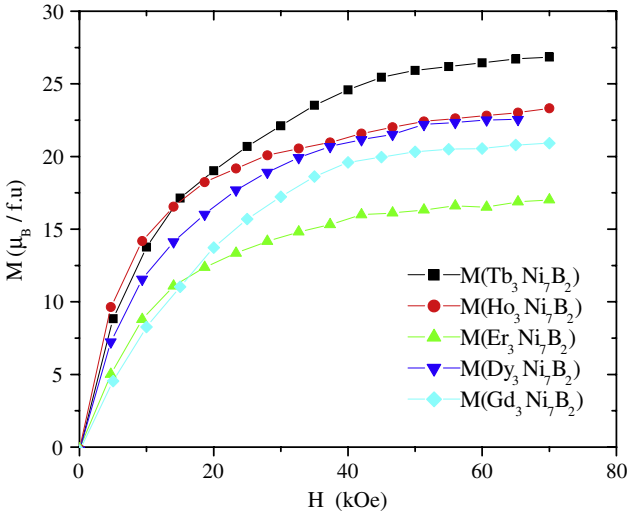

Figure 9. Magnetization isotherms at 4.2 K in fields up to 70 kOe.

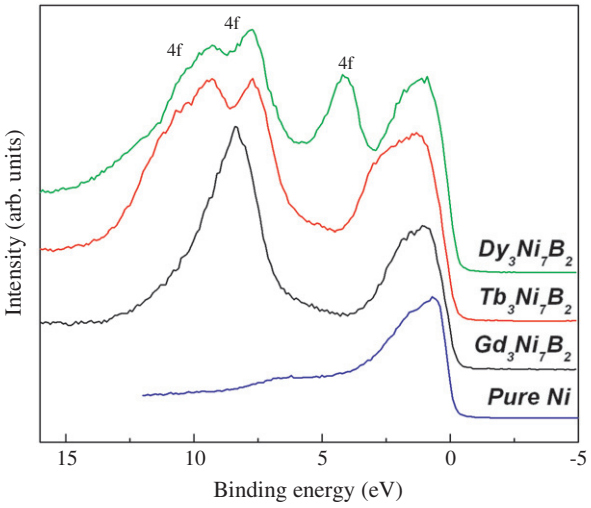

Figure 8. The XPS valence bands and of 4f states for $R_3Ni_7B_2$ (R = Gd, Tb, Dy) compounds and pure nickel.

we determined their positions. These were shown to be located at the same binding energies as in Dy metal. Similar results were suggested from the inspection of valence bands in other studied compounds. As in the case of R metals [17], the crystal field is well shielded by the valence electrons and it is negligible as compared with the separation of multiplet states. The small shifts in Dy4f line positions may be correlated with minor changes in the shielding which result from modification in the electron concentrations, as a result of alloying.

5. Magnetic measurements

The magnetization isotherms, obtained at 4.2 K, are plotted in figure 9. Even in a field of 70 kOe, the saturation has been not attained. The saturation moments obtained by extrapolation of the measured values, to $H^{-1} \rightarrow 0$, are given in table 2. The magnetic contributions of nickel are smaller than $\cong 0.50\ \mu_B$ per formula unit and are oriented antiparallel to the R moment, as shown by band structure calculations. Consequently, the contributions of rare-earths to magnetization are dominant. The saturation magnetizations for $R_3Ni_7B_2$ with R = Gd and Tb, which have Curie temperatures above 30 K, are close to the expected $g_J J$ values, namely $M_{Gd} = 7\ \mu_B$ and $M_{Tb} = 9\ \mu_B$. The differences between expected magnetizations and measured values increase as the Curie temperatures, T_C, are lowered. At 4.2 K, where the magnetizations were determined, the T/T_C values are of $\cong 0.20$ (R = Dy), 0.36 (R = Ho), and 0.60 (R = Er). At these reduced temperatures, a decrease of magnetizations as compared to the value at 0 K is expected, due to thermal effects. As an example, by using the molecular field approximation, in the case of $Er_3Ni_7B_2$, at $T/T_C \cong 0.6$, the expected magnetization is $\cong 19.2\ \mu_B$/f.u. close to the experimental value of 18.7 μ_B/f.u. Thus, the lower saturation magnetizations as compared to $g_J J$ values can be correlated with thermal effects.

The coefficients of magnetic hardness, a, in non-S-state rare-earth compounds, decrease in the sequence Tb (0.8), Dy (0.7), Ho (0.67), and Er (0.57), suggesting a decrease of the anisotropy as the atomic number of the R element increases. The Curie temperatures, T_C, are rather low—table 2—and follow approximately a De Gennes relation.

The temperature dependences of the reciprocal susceptibilities, χ^{-1}, follow a Curie–Weiss behaviour, described by the relation $\chi^{-1} = C^{-1}(T - \theta)$—figure 10. We denoted by C the Curie constant and θ is the paramagnetic Curie temperature. The θ values are somewhat higher than the ferromagnetic ones.

The Curie constants, C, are greater than those characteristic for free R^{3+} ions. This suggests that nickel atoms contribute also to the Curie constants. Assuming that the Curie constants of rare-earths are the same as those of free R^{3+} ions, according to the additive law of susceptibilities, we determined the contributions of Ni, C_{Ni}, at C values as well as the effective nickel moments—table 2. Effective nickel moments of $1.32 \pm 0.25\ \mu_B$ were obtained.

Table 2. Saturation magnetizations at 4.2 K, M_s, Curie temperature, T_C, paramagnetic Curie temperatures, θ, Curie constants, C, and effective nickel moments, μ_{eff}.

Composition	M_s (μ_B/f.u.)	T_C (K)	C (emu K mol^{-1})	μ_{eff} (μ_B/Ni atom)	θ (K)
$Gd_3Ni_7B_2$	20.9	38.5	25.80	1.54	39.4
$Tb_3Ni_7B_2$	26.6	30.6	37.60	1.58	31.2
$Dy_3Ni_7B_2$	25.5	22.8	43.67	1.31	22.9
$Ho_3Ni_7B_2$	24.0	14.6	43.25	1.11	14.7
$Er_3Ni_7B_2$	18.7	7	35.58	1.21	8.4

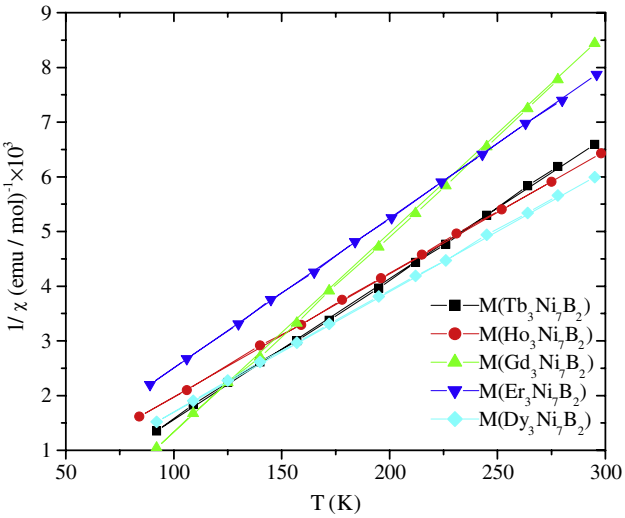

Figure 10. Thermal variations of reciprocal susceptibilities.

6. Discussion

The band structure calculations show the presence of very small nickel magnetic moments, at 0 K, in an antiparallel orientation to the rare-earth moments. The contributions of all nickel atoms are smaller than 2% from saturation magnetizations per formula unit. Thus, the compounds can be considered as nearly ferromagnets. There are induced polarizations on the R5d bands, in addition to those of the Ni3d bands. The exchange interactions can be described as being of 4f–5d–3d type between rare-earths and nickel and R5d–R5d type between rare-earths. Due to the small polarizations of R5d and Ni3d bands, the Curie temperatures of the compounds are rather low. We suspect that the RKKY interactions have small contributions in the present system as shown previously in the $DyNi_{5-x}Al_x$ system [18]. These involve higher Curie temperatures than those above-determined, as, for example, evidenced in RAl_x ($x = 2, 4$) compounds [19].

In the paramagnetic range, effective nickel moments of 1.33 ± 0.25 μ_B were determined. Thus, according to the paramagnetic data, the Ni3d band is not completely filled, having an approximate $3d^9$ configuration. This agrees with the results of XPS measurements, where the presence of a 6 eV satellite at room temperature confirms the existence of unoccupied Ni3d states.

The magnetic behaviour of nickel, which shows a nearly nil saturation moment at 0 K and an effective moment above the Curie temperature, can be analysed in models that take into account the electron correlation effects in the d band as a spin fluctuation model [20] or dynamical mean field theory [21]. These models reconcile the dual character of the electron which, as a particle, requires a real space description and as a wave, a momentum space description. The spin fluctuation model considers the balance between the frequencies of longitudinal spin fluctuations, which are determined by their life-time and of transverse fluctuations that are of thermal origin. These effects lead to the concept of temperature induced moments. For a nearly ferromagnet, as Ni is in the present system, the average amplitude of spin fluctuations increases, in a limited temperature range above the Curie points, and it reaches an upper limit determined by the charge neutrality condition. At higher temperatures, a Curie–Weiss behaviour is predicted, as for systems having localized moments. In this case the moments are localized in q-space. The determined effective Ni moments (1.33 ± 0.25 μ_B/atom) are smaller than the characteristic value for Ni^{2+} ions, considering only the spin contribution (2.83 μ_B/atom). This behaviour can be correlated with the hybridization effects, resulting in the diminution of the number of 3d holes in the spin minority band, as suggested also by the decrease of the 6 eV satellite line intensity as compared to that of pure nickel. This behaviour is similar to that observed in $LaNi_{5-x}Al_x$ [22] or $TbNi_{5-x}Al_x$ [23] systems.

The magnetic behaviour of nickel in the present system, may also be described in the dynamical mean field theory (DMFT) combined with the standard LDA band calculation (LDA + DMFT) [21, 24]. In this model [24], for an itinerant electron system, the time dependence of the correlation function results in a temperature dependence of the average amplitude of spin fluctuation. Fluctuating moments and atomic-like configurations are large at short timescales. The moment is reduced at longer timescales, corresponding to a more band-like less correlated electronic structure near the Fermi level. By using a numerically exact quantum scheme in LDA + DMFT it was possible to reproduce the 6 eV satellite DOS spectrum of Ni, at $T = 0.9T_C$ [24]. The satellite was shown to have a greater spin–up contribution. The lower 6 eV satellite line intensity as compared to nickel is in agreement with the diminution of the number of Ni3d holes in the $R_3Ni_7B_2$ system as evidenced by magnetic measurements at $T > T_C$.

We conclude that the exchange interactions in $R_3Ni_7B_2$ can be described by the 4f–5d–3d model. The nickel moments, at 0 K, are very small and are oriented antiparallel to the rare-earth ones. In the paramagnetic range, nickel has an effective moment, suggesting an atomic configuration close to

$3d^9$. The magnetic behaviour of nickel in the present system can be analysed in a model which takes into account electron correlations effects in d bands.

References

[1] Burzo E, Chelkovski A and Kirchmayr H R 199 *Landolt Börnstein Handbuch* vol III/19d2 (Berlin: Springer)
[2] Gignoux D, Givord D and Del Moral A 1976 *Solid State Commun.* **19** 891
[3] Burzo E, Chioncel L and Costina I 2001 *Mater. Sci. Forum* **373–376** 696
[4] Burzo E, Chioncel L, Costina I and Chiuzbaian S 2006 *J. Phys.: Condens. Matter* **18** 4861
[5] Burzo E and Chioncel L 2004 *J. Opt. Adv. Mater.* **6** 917
Burzo E 2004 *Mol. Cryst. Liq. Cryst.* **417** 491
[6] Yano K, Tanaka Y, Matsumoto I, Umehara I, Sato K, Adachi H and Kawata H 2006 *J. Phys.: Condens. Matter* **18** 6891
[7] Kuz'ma Yu B and Chaban N F 1980 *Dopov. Akad. Nauk Ukr. SSR* A **88** 91
[8] Anderson O K 1975 *Phys. Rev.* B **12** 3060
Anderson O K and Jepsen O 1984 *Phys. Rev. Lett.* **53** 2571
[9] Anderson O K and Saha-Dasgupta T 2000 *Phys. Rev.* B **62** R16219
Anderson O K and Saha-Dasgupta T 2003 *Bull. Mater. Sci.* **26** 19
[10] Anisimov V I, Aryasetiawan F and Lichtenstein A I 1997 *J. Phys.: Condens. Matter* **9** 767
[11] Larson P, Lambrecht W R L, Chantis A and Van Scilfgaarde M 2007 *Phys. Rev.* B **75** 045114
[12] Yang I, Savrasov S Y and Kotliar G 2001 *Phys. Rev. Lett.* **87** 216495
Burzo E, Crainic T, Neumann M, Chioncel L and Lazar C 2005 *J. Magn. Magn. Mater.* **290/291** 371
[13] Vincent Crist B 1999 *Handbook of Monochromatic XPS Spectra* vol 1 (California: XPS International INC)
[14] Campagna M, Wertheim G K and Baer Y 1979 *Topics in Applied Physics* vol 27 (Berlin: Springer) p 217
[15] Baer Y and Lang J K 1979 *J. Appl. Phys.* **50** 7485
[16] Lang J K, Baer Y and Cox P A 1981 *J. Phys. F: Met. Phys.* **11** 121
[17] Huffner St 1995 *Photoelectron Spectroscopy* (Berlin: Springer)
[18] Burzo E, Chiuzbaian S G, Neumann M, Valeanu M, Chioncel L and Creanga I 2002 *J. Appl. Phys.* **92** 7362
[19] Buschow K H J 1979 *Rep. Prog. Phys.* **42** 1373
[20] Moriya T 1991 *J. Magn. Magn. Mater.* **100** 201
[21] Georges A, Kotliar G, Krauth W and Rosenberg M J 1996 *Rev. Mod. Phys.* **68** 13
[22] Burzo E, Chiuzbaian S G, Neumann M and Chioncel L 2002 *J. Phys.: Condens. Matter* **14** 8057
Burzo E 2007 *J. Opt. Adv. Mater.* **9** 1113
[23] Burzo E, Crainic T, Neumann M, Chioncel L and Lazar C 2005 *J. Magn. Magn. Mater.* **290/291** 571
[24] Lichtenstein A I, Katsnelson M and Kotliar G 2001 *Phys. Rev. Lett.* **87** 067205